Letter | Editors' Suggestion

Impact of cross and main diffusion coefficients on symmetry breaking in nonreactive diffusion systems

Berin Šeta and Jon Spangenberg
Department of Civil and Mechanical Engineering, Technical University of Denmark, Koppels Allé, Kgs. Lyngby 2800, Denmark

Mounir M. Bou-Ali
Mechanical and Manufacturing Department, Mondragon University, Loramendi 4, Mondragon 20500, Spain

Valentina Shevtsova*
Mechanical and Manufacturing Department, Mondragon University, Loramendi 4, Mondragon 20500, Spain and Ikerbasque, Basque Foundation for Science, Bilbao 48011, Spain

(Received 9 December 2024; accepted 18 July 2025; published 25 September 2025)

Diffusion-triggered convection can occur in a gravitationally stable system of two superimposed mixtures. As instability develops, two distinct patterns may emerge: double-diffusive (DD) or diffusion-layer convection (DLC). Traditionally, nonsymmetric patterns above and below the interface were thought to require chemical reaction. We show that symmetry can be broken by composition-dependent diffusion, with or without cross diffusion. Furthermore, only the composition-dependent cross diffusion can lead to a range of coexisting patterns and provide new insights into staircase instability.

DOI: 10.1103/yr2z-b9px

Hydrodynamic instability of miscible interfaces arises in various applications where two fluids come into contact. In diffusive multicomponent mixtures, even in gravitationally stable systems, instability can be triggered by opposing contributions to the density profile. Common examples of such contributions can be temperature and concentration [1], different diffusion rates of two species [2,3], or chemical reactions that alter the density of the solution [4–7].

If the lower (denser) fluid diffuses faster than the upper (less dense), the instability occurs in the form of double-diffusive fingering (DD) [3], or if the upper diffuses faster than the lower, then instability emerges in the form of diffusive-layer convection (DLC) also called overstability [8]. It has been widely assumed that in nonreactive miscible fluids, convective patterns develop symmetrically above and below the initial contact line, and only the presence of a chemical reaction is capable of breaking this symmetry [6,9,10]. Although symmetric patterns are central to double-diffusion phenomena, this assumption is challenged in certain cases, and recent studies on mixtures with composition-dependent coefficients [11] and/or ternary mixtures with cross diffusion lead to more complex flow organization [12,13]. A complex spatiotemporal evolution of composition can then set in due to the highly nonlinear nature of the underlying dynamics.

In this Letter, we address the conditions under which the main and cross diffusion coefficients in a ternary mixture can result in non-symmetric convective instability patterns on either side of an initially stable interface. The system consists of two layers of the same ternary mixture but with different compositions, where mutual diffusion generates a transient concentration gradient. We have developed a theoretical and numerical model to predict and follow the evolution of these instabilities. We demonstrate that when the main or cross diffusion coefficients (or both) are composition dependent, instabilities such as double diffusion (DD) or diffusion layer convection (DLC) can emerge asymmetrically on either side of the interface—an outcome previously thought to be exclusive to systems involving chemical reactions. In the ternary system, they can coexist, and their coexistence can give rise to multilayered structures resembling thermohaline staircases in the ocean [14]. Furthermore, we reveal the transient nature of the buoyancy-driven instability, where a system initially in a stable region may temporarily intersect the stability boundary and trigger DD or DLC instability. We explain how, by incorporating composition-dependent cross diffusion, both its value and spatial profile can be used to control the location and amplitude of convective motion.

To gain insight into these previously unexplored phenomena, we consider a ternary mixture with mass fraction of components i by c_i $(i = 1, 2)$, $(c_1 + c_2 + c_3 = 1)$. Although the correct notation for mass fraction is w, we use c for reader convenience, as is common in fluid dynamics. The species occupy a cell of size $L_x \times L_y$, where the y axis is vertical and $\mathbf{g} = (0, -g)$. At the initial time of contact, $t = 0$, the mixtures are separated by a sharp boundary at $y = y_0$, and the density profile between the two layers of solutions follows a step

*Contact author: x.vshevtsova@mondragon.edu

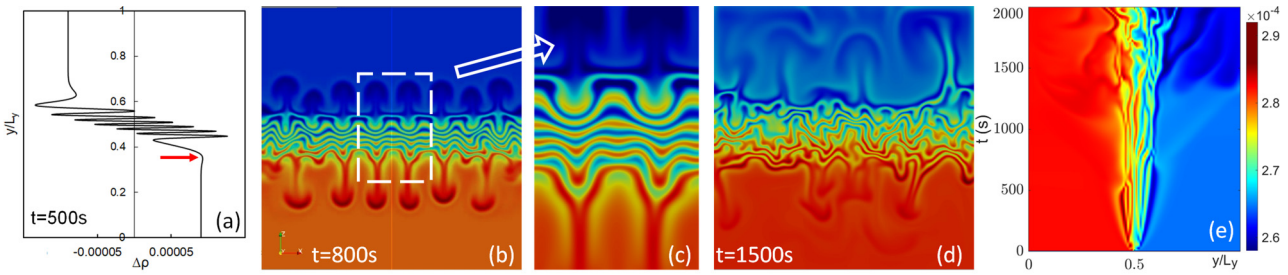

FIG. 1. Intriguing instabilities in a ternary mixture triggered by oscillating cross diffusion with $\tilde{D}_{12} = 0.5\sin(500\,c_2)$, while the other coefficients are constant $\tilde{D}_{11} = 1.1$, $\tilde{D}_{21} = 0$, $\tilde{D}_{22} = 1.0$ where $\tilde{D}_{ij} = D_{ij}/D_0$ and $D_0 = 10^{-9}\mathrm{m}^2/\mathrm{s}$. (a) The density profile at $t = 500\,\mathrm{s}$ indicates the emergence of seven layers of distinct instability patterns in the central part. The red arrow suggests a potential DLC instability at the bottom. (b), (c) The 2D density field at $t = 800\,\mathrm{s}$ and its magnification highlight the multilayer instability in the form of fingers. (d) The emergence of DLC near the top and bottom limits the expansion of the multilayer fingering instability. (e) The space-time map along the central vertical line confirms that the DLC patterns constrain the multilayer finger system at later times. The initial composition of the bulk mixtures and the associated D_{ii} values are taken from the rectangle in Fig. 3.

function. The initial species compositions are $c_i^t(t=0) = c_{i0}^t$ when $y > y_0$, and $c_i^b(t=0) = c_{i0}^b$ when $y < y_0$. The density of the mixture, ρ, is a linear function of the mass fractions

$$\rho = \rho_r[1 + \beta_{c1}(c_1 - c_{1r}) + \beta_{c2}(c_2 - c_{2r})], \tag{1}$$

where $\beta_{c_i} = (1/\rho)(\partial\rho/\partial c_i)|_{c_{i0}}$, and $c_{ir} = (c_{i0}^t + c_{i0}^b)/2$ and $\rho_r = (\rho_0^t + \rho_0^b)/2$ are the reference values. No-slip velocity and impermeability conditions for species are imposed on all boundaries. The spatiotemporal dynamics of this system is described by the Navier-Stokes and mass transfer equations in the Boussinesq approximation [15]:

$$\mathrm{div}\,\vec{V} = 0, \tag{2}$$

$$\frac{\partial\vec{V}}{\partial t} + \vec{V}\cdot\nabla\vec{V} = -\frac{1}{\rho_r}\nabla p + \nu\Delta\vec{V} + \vec{g}\rho^*, \tag{3}$$

$$\frac{\partial c_1}{\partial t} + \vec{V}\cdot\nabla c_1 = \nabla\cdot(D_{11}\nabla c_1) + \nabla\cdot(D_{12}\nabla c_2), \tag{4}$$

$$\frac{\partial c_2}{\partial t} + \vec{V}\cdot\nabla c_2 = \nabla\cdot(D_{21}\nabla c_1) + \nabla\cdot(D_{22}\nabla c_2). \tag{5}$$

Here $\vec{V}$ is the velocity, p is the difference between total and hydrodynamic pressure, ν is the kinematic viscosity, and $\rho^* = \rho - \rho_r$. Hereafter, the notations D_{ij} and D_{ii} will be used for the full set and the main terms of the diffusion matrix, respectively.

To illustrate the powerful role of cross diffusion in governing instabilities, we first examine the thought-provoking scenario in which the cross diffusion coefficient D_{21} is set to zero, while D_{12} is periodic, exhibiting seven oscillations with constant amplitude around zero value. The initial density distribution follows a step function. Nonlinear simulations of Eqs. (2)–(5) reveal that, over time, the diffusive system develops seven layers of fingering instabilities contained by DLC from the bottom, as illustrated in Fig. 1. Interestingly, since the fingers develop faster than the DLC, the DD instability begins at the bottom from the preceding layer. The formation of large fingers at the leading edges in the upper and lower regions, along with a set of smaller ones between them, is illustrated by the 2D density fields in panels (b) and (c) at $t = 800\,\mathrm{s}$. At the later times, the DLC instability emerges and takes over at the top and bottom, while the multilayered finger structure in the center remains active. The last panel (e) presents a space-time map along the vertical line at $x/L_x = 0.5$, highlighting the evolution of the steplike fingering system. It also illustrates that the multilayers are spatially constrained by the DLC from both sides until the end of the observation. Given that diffusion coefficients depend on temperature and composition, this scenario is not entirely theoretical as it will be shown later. We suggest that such multilayer instability may resemble thermohaline staircases in oceans, which are characterized by steplike structures observed in vertical temperature and salinity profiles [14]. Somewhat similar effects might occur in biological systems involving nutrient and oxygen transport and in the Earth's mantle, where variations in chemical diffusion lead to layered convection.

To predict the sensitivity of instability patterns to variations of D_{ij}, we have developed an analytical solution in the case of constant diffusion coefficients (cf. the Supplemental Material [16]). The output of this solution defines the system stability, which can be classified into four categories: unstable, in the form of Rayleigh-Taylor instability, i.e., $d\rho/dz > 0$, stable, DD, and DLC. The neutral stability curve, separating the unstable region from the others, is determined without solving the diffusion equations as

$$\Delta\rho = \Delta c_1\beta_{c1} + \Delta c_2\beta_{c2} = 0. \tag{6}$$

The conditions to occur the finger instability (DD) and DLC, respectively, are determined as

$$-1 \geqslant \frac{\Delta\rho_2}{\Delta\rho_1} \geqslant -\frac{\sqrt{(D_{22}D_{11} - D_{12}D_{21})} + D_{22} - \frac{\beta_1}{\beta_2}D_{21}}{\sqrt{(D_{22}D_{11} - D_{12}D_{21})} + D_{11} - \frac{\beta_2}{\beta_1}D_{12}}, \tag{7}$$

$$-1 \geqslant \frac{\Delta\rho_2}{\Delta\rho_1} \geqslant \frac{2\hat{D}_2 - 2D_{11} - 2(\beta_2/\beta_1)D_{21}}{2\hat{D}_1 - 2D_{11} + 2(\beta_1/\beta_2)D_{12}}. \tag{8}$$

Here $\hat{D}_1, \hat{D}_2$ are the eigenvalues of the diffusion matrix. The division by $\Delta\rho_1$ or $\Delta\rho_2$ is interchangeable.

These inequalities can be applied to a system where the diffusion coefficients D_{ij} are constant within each layer but differ between the top and bottom layers, representing different compositions of a ternary mixture. Thus, they enable tracking how the instability type changes with composition.

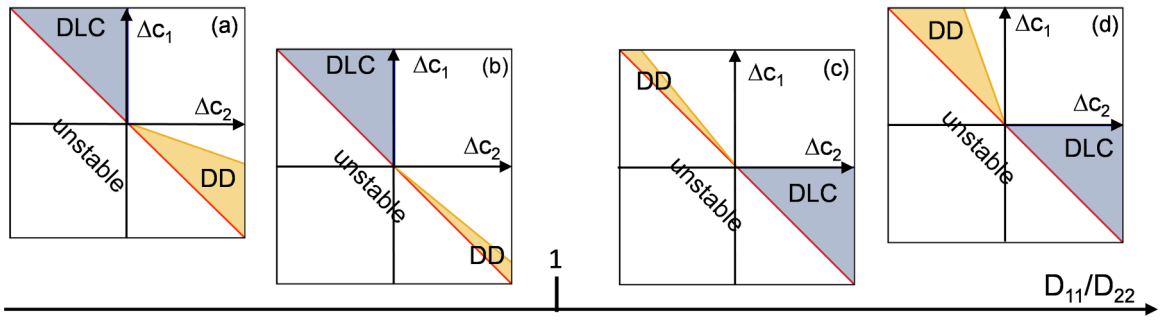

FIG. 2. A shift in the location of instability regions in the $(\Delta c_1, \Delta c_2)$ plane [equivalent to the $(\Delta\rho_1, \Delta\rho_2)$ plane] with variation in the diffusion coefficient difference: (a), (b) $D_{22} > D_{11}$, and (c), (d) $D_{22} < D_{11}$. Here cross diffusion is neglected, $\beta_{c1} = \beta_{c2}$. Each of the two lines bounding the region of DD or DLC instability regions is determined by one of the two inequalities in Eqs. (7) or (8), respectively.

By selecting different initial compositions on either side of the initial contact line and associating them with the corresponding diffusion coefficients, the above expressions allow us to construct a stability map (as in Fig. 2). It is important to note that these stability maps may differ between the top and bottom layers due to the different diffusion coefficients, potentially resulting in DD (DLC) in the top layer and DLC (DD) in the bottom. This leads to the conclusion that composition-dependent D_{ij} inherently breaks the symmetry of patterns relative to the initial contact line. However, when D_{ij} are equal in both layers, the patterns are symmetric, as previously discussed in the literature [9,10].

To further investigate the emergence and shift of various instabilities with composition, we temporarily omit cross diffusion and assume $\beta_{c1} = \beta_{c2}$. In this case, the exchange of instability types depends on whether D_{11} or D_{22} is larger. Figure 2 shows how the location of the instabilities shifts as the ratio D_{11}/D_{22} changes, focusing independently on the top (bottom) layer. As the ratio approaches unity, the region where fingering occurs shrinks [compare panels (a) and (b)]. When D_{11} exceeds D_{22}, the fingering region reappears but in a different plane [panels (c) and (d)]. The DLC forms when either Δc_1 or Δc_2 is zero, indicating the absence of concentration gradients across the interface.

The inclusion of cross diffusion with constant coefficients does not fundamentally alter the overall structure of the stability map; however, it significantly affects the parameter space where instabilities arise. Cross diffusion can expand or contract these instability regions and swap the locations of DD and DLC patterns. Stability exchange typically occurs when the sign of one of the cross diffusion coefficients changes, though this is not always the case. The exchange tends to occur more consistently when the other cross diffusion coefficient is close to zero.

To sum up, the discussion above suggests that the instability is inherently transient. Even small variations in diffusion properties can cause the system to cross stability boundaries, triggering instabilities that might not have been anticipated under the initial state.

Now we turn to the analysis of a real ternary mixture, considering two layers of the toluene (T)-methanol (M)-cyclohexane (Ch) mixture with slightly different compositions. The thermophysical properties of the mixture have been studied in both ground-based and orbital laboratories and have revealed that, for some range compositions, the cross diffusion coefficient can be three times larger than one of the main diffusion coefficients [24–28].

Moreover, at certain locations on the Gibbs triangle, even small changes in composition cause significant variations in both cross diffusion terms and even change their signs. It is the region that attracts our attention here. The composition dependence of all diffusion coefficients on c_2 was taken from the experiment [24,25] in the region, where the effect of c_1 is negligible, see Fig. 3(a).

Nonlinear simulations with variable during the diffusion process $D_{ij}(c)$, cf. Fig. 3(b), reveals the emergence of previously unreported, diverse, nonsymmetric instability patterns at the top and bottom layers, indicative of the complex behavior introduced by the composition-dependent diffusion. To demonstrate its critical impact, we have selected three distinct scenarios for further discussion; cf. Fig. 4. First, we

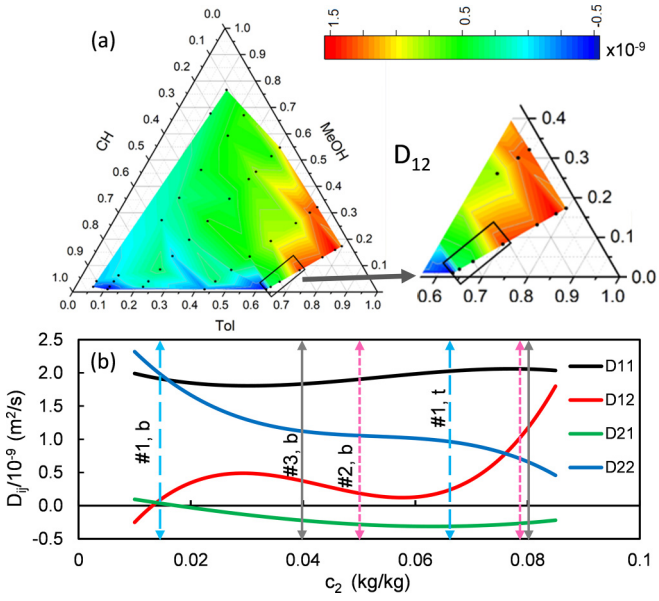

FIG. 3. (a) cross diffusion coefficient D_{12} of the (T)-(M)-(Ch) mixture on the Gibbs triangle. The dots mark the compositions where all D_{ij} coefficients were measured [24,25]. The compositions of the mixture are given in [kg/kg]. (b) The dependence of D_{ij} on c_2 within the small rectangle above. The vertical lines of the same color represent the initial c_2 and corresponding D_{ij} values at the top and bottom layer for the cases discussed in Fig. 4.

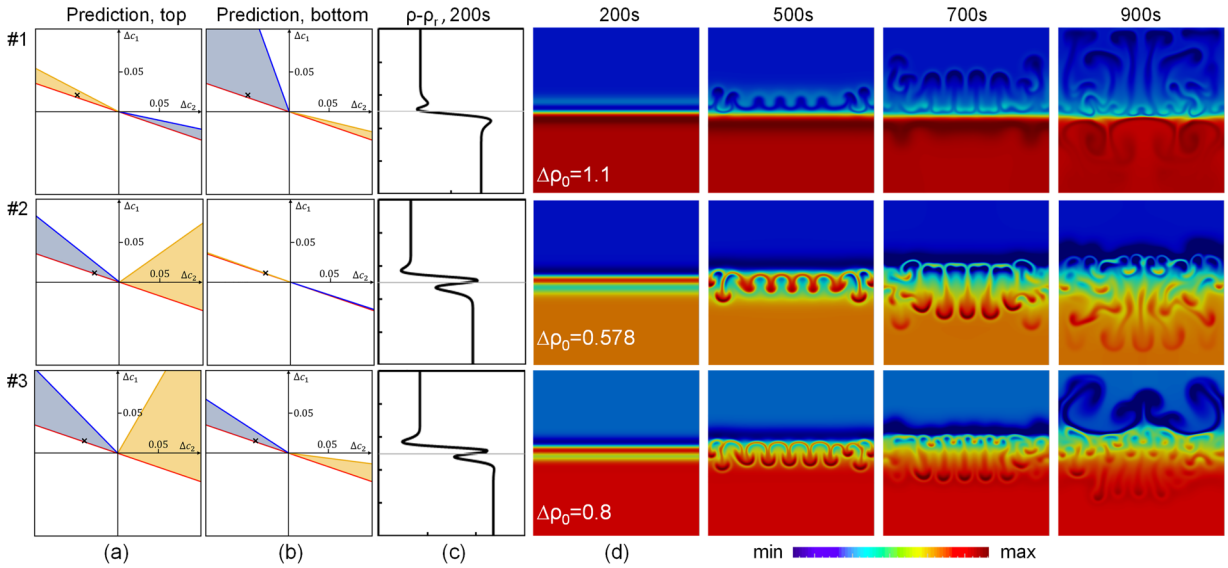

FIG. 4. Dynamic behavior of the Tol-Meth-Ch system with constant across the layer and composition-dependent diffusion coefficients. Panels (a) and (b) show the predicted instability patterns based on Eqs. (7) and (8) for constant D_{ij} within each layer; (c) shows the density profiles at $t = 200$s, while (d) illustrates the spatiotemporal evolution of 2D density fields in systems where D_{ij} varies during the diffusion process as shown in Fig. 3.

construct stability maps for both layers (top and bottom) based on Eqs. (7) and (8), for the (T)-(M)-(Ch) mixture, shown in panels (a) and (b). They predict instabilities when diffusion coefficients are constant across a layer but differ between the top and bottom layers. Such predictions are useful in practice when the $D_{ij}(c)$ values are poorly known. The crosses indicate the initial concentration field (Δc_1 and Δc_2), serving as a key reference for the scenarios under discussion.

According to the predictions, in scenario 1, if D_{ij} remains constant, finger instability is expected at the top layer, while DLC occurs at the bottom. At $t = 200$ s (Fig. 4), the density profile shows that introducing variable diffusion coefficients does not alter these predictions. In the top layer, nonlinear dynamics reveal the formation of regular upward fingers, each featuring a mushroom head, which propagate with a constant wavelength without generating new fingers along the boundary until $t = 800$ s. Below the contact line, where D_{11} is initially large [cf. Fig. 3(b)], a depletion zone develops as toluene diffuses outward without being replaced by the slower-moving methanol from the top. Over time, the DLC convective pattern establishes in the lower region, preventing the fingers from extending beneath the contact line. As predicted by our maps of stability, the instabilities differ above and below the initial interface, demonstrating the coexistence of different instability types and the breaking of symmetry around the interfacial point.

In scenario 2, the system starts in the DLC region at the top, while the bottom remains in a stable region where the instability threshold is extremely narrow for the initial composition at the bottom ($c_2 = 0.047$). The system is highly sensitive to small variations in c_2: for $c_2 = 0.04$, DLC occurs; at 0.047, the system is stable; at 0.05, finger instability emerges; and beyond 0.07, DLC reappears; see Movie 1. As diffusion begins, the c_2 value at 0.047 shifts to 0.05, causing the system to cross the stability boundary into the DD region. The 2D density maps reveal sinking fingers developing downward, while their flat-tipped bases move upward, split, and generate new sinking fingers at $t \sim 800$ s. DLC sets in more slowly, emerging at $t \sim 1000$ s once the fingers have occupied most of the cell. The stability map initially shows a stable bottom region but also reveals the system's temporal behavior during diffusion, predicting the formation of fingers, see Movie 1. If diffusion coefficients remained constant during mixing, the fingers would not form, as the stability map would be static.

In scenario 3, both the top and bottom layers start in the DLC region. Nevertheless, the system crosses the stability boundary, and fingers form across the initial contact line. These fingers propagate downward with mushroom-shaped heads and upward as flat-tipped fingers, which split around $t = 600$ s. DLC then dominates at the top, preventing further upward spread of the fingers. At the bottom, the predicted DLC convection is significantly delayed. This delay is due to the profile of $D_{12}(c_2)$, which approaches zero, slowing the diffusion of toluene, which is present in excess at the bottom. Eventually, a three-layer system forms, where the central finger zone is confined by DLC zones above and below, highlighting the dynamic interplay between diffusion and convection, see Movie 2. This scenario, observed in real ternary mixture, closely resembles the multilayered instability discussed above. Note that prediction based on constant diffusion coefficients entirely misses the formation of the DLC-DD-DLC triple layer, which is observed for the first time in the literature.

The emergence of nonsymmetric instability patterns in the top and bottom layers challenges long-held assumptions about symmetry in nonreactive systems. Previously considered mutually exclusive, different instability types can occur simultaneously. Beyond symmetry breaking, this study reveals several unobserved phenomena arising from composition-dependent diffusion, cross diffusion, or both. These include the transient nature of double-diffusion instabilities and the simultaneous presence of three instability types. Moreover,

diffusion-convection interactions in multicomponent mixtures can generate and sustain complex, multilayered instability patterns, highlighting the profound role of cross diffusion effects. Scenario 3 reveals that diffusion itself can regulate the timing of convection, providing key insights into the transient behavior of such systems. These findings deepen our understanding of instabilities in multicomponent systems and open possibilities for practical applications.

B.S. and J.S. acknowledge the support of the Independent Research Fund Denmark (DFF) (Contract No. 0171-00115B). M.M.B.-A. and V.S. acknowledge the Basque Government for funding the MMASINT project (KK-2023/00041, Elkartek Programme), and the Research Group Programme (IT1505-22) and the Spanish Government for the PID2023-149539NB-C33 and PCI2024-155071-2 projects, funded by MCIN/AEI.

Data availability. The data that support the findings of this article are not publicly available upon publication because it is not technically feasible and/or the cost of preparing, depositing, and hosting the data would be prohibitive within the terms of this research project. The data are available from the authors upon reasonable request.

[1] M. E. Stern, Tellus **12**, 172 (1960).
[2] C. A. Cooper, R. J. Glass, and S. W. Tyler, Water Resour. Res. **33**, 517 (1997).
[3] S. E. Pringle and R. J. Glass, J. Fluid Mech. **462**, 161 (2002).
[4] F. Brau, G. Schuszter, and A. De Wit, Phys. Rev. Lett. **118**, 134101 (2017).
[5] M. A. Budroni, V. Upadhyay, and L. Rongy, Phys. Rev. Lett. **122**, 244502 (2019).
[6] A. De Wit, Annu. Rev. Fluid Mech. **52**, 531 (2020).
[7] A. De Wit, K. Eckert, and S. Kalliadasis, Chaos: An Interdisciplinary J. Non. Sci. **22**, 037101 (2012).
[8] P. Vitagliano, C. Volpe, and V. Vitagliano, J. Solution Chem. **13**, 549 (1984).
[9] C. Almarcha, P. M. J. Trevelyan, P. Grosfils, and A. De Wit, Phys. Rev. Lett. **104**, 044501 (2010).
[10] M. Budroni and F. Rossi, Phys. Chem. Chem. Phys. **26**, 29185 (2024).
[11] D. A. Bratsun, V. O. Oschepkov, E. A. Mosheva, and R. R. Siraev, Phys. Fluids **34**, 034112 (2022).
[12] M. A. Budroni, L. Lemaigre, A. De Wit, and F. Rossi, Phys. Chem. Chem. Phys. **17**, 1593 (2015).
[13] A. Vailati, B. Šeta, M. Bou-Ali, and V. Shevtsova, Int. J. Heat Mass Trans. **229**, 125705 (2024).
[14] D. Walsh and B. Ruddick, J. Phys. Oceanography **25**, 348 (1995).
[15] B. Šeta, A. Errarte, D. Dubert, J. Gavaldà, M. M. Bou-Ali, and X. Ruiz, Acta Astronaut. **160**, 442 (2019).
[16] See Supplemental Material at http://link.aps.org/supplemental/10.1103/yr2z-b9px for derivations of limits from Eqs. (7) and (8) using the analytical solution for ternary mixtures are shown; These limits are then used in the construction of graphs of stability shown in Figs. 2 and 4; and which includes Refs. [17–23].
[17] R. Taylor and R. Krishnar, *Multicomponent Mass Transfer*, 2nd ed. (Wiley Series in Chemical Engineering, 1993).
[18] S. Kozlova, A. Mialdun, I. Ryzhkov, T. Janzen, J. Vrabec, and V. Shevtsova, Phys. Chem. Chem. Phys. **21**, 2140 (2019).
[19] H. Fujita and L. J. Gosting, J. Am. Chem. Soc. **78**, 1099 (1956).
[20] B. Šeta, Ph.D. thesis, Universitat Rovira i Virgili, Tarragona, 2020.
[21] T. J. McDougall and J. S. Turner, Nature (London) **299**, 812 (1982).
[22] T. J. McDougall, J. Fluid Mech. **126**, 379 (1983).
[23] D. G. Miller and V. Vitagliano, J. Phys. Chem. **90**, 1706 (1986).
[24] T. Grossmann and J. Winkelmann, J. Chem. Eng. Data **54**, 405 (2009).
[25] T. Grossmann and J. Winkelmann, J. Chem. Eng. Data **54**, 485 (2009).
[26] A. Mialdun, I. Ryzhkov, O. Khlybov, T. Lyubimova, and V. Shevtsova, J. Chem. Phys. **148**, 044506 (2018).
[27] B. Seta, A. Errarte, I. I. Ryzhkov, M. M. Bou-Ali, and V. Shevtsova, Phys. Fluids **35**, 021702 (2023).
[28] B. Seta, A. Errarte, A. Mialdun, I. I. Ryzhkov, M. M. Bou-Ali, and V. Shevtsova, Phys. Chem. Chem. Phys. **25**, 15715 (2023).